Crystal structure and physical properties of Yb_2In and $Eu_{2-x}Yb_xIn$ alloys

F. Guillou,[1] H. Yibole,[1,*] R. Hamane,[2] V. Hardy,[2] Y. B. Sun,[3] J. J. Zhao,[3] Y. Mudryk,[4] and V. K. Pecharsky[4,5]

[1]*Inner Mongolia Key Laboratory for Physics and Chemistry of Functional Materials, College of Physics and Electronic Information, Inner Mongolia Normal University, 81 Zhaowuda Road, Hohhot, 010022, Inner Mongolia, China*

[2]*Normandie Univ, ENSICAEN, UNICAEN, CNRS, CRISMAT, 14000 Caen, France*

[3]*Key Laboratory of Magnetism and Magnetic Materials at Universities of Inner Mongolia Autonomous Region, Department of Physics, Baotou Teacher's College, Baotou 014030, China*

[4]*Ames Laboratory US Department of Energy, Iowa State University, Ames, Iowa 50011-2416, USA*

[5]*Department of Materials Science and Engineering, Iowa State University, Ames, Iowa 50011-1096, USA*

(Received 25 June 2020; revised 11 August 2020; accepted 10 September 2020; published 5 October 2020)

While binary RE_2In, where RE = rare earth, have been reported a few decades ago, recent investigations revealed intriguing new physical insights. For instance, the discovery of a nearly ideal first-order ferromagnetic transition in Eu_2In calls for further exploration of structures and properties of RE_2In, in particular for the least-documented RE = Eu and Yb cases. Here, we investigate $Eu_{2-x}Yb_xIn$ pseudobinaries with nominal values of $x = 0.25$, 0.5, 0.75, 1, 1.5, 2 by powder x-ray diffraction (including as function of temperature from 100 to 375 K for Yb_2In), magnetization (5–300 K), as well as electrical resistivity (5–300 K) and calorimetric (2–150 K) measurements for Yb_2In. Compared to other RE, Yb or Eu always raise challenging questions linked to their valence states. From average atomic volume, Yb is anticipated to be divalent in Yb_2In, at least between 100 and 375 K, which is in line with the absence of $4f$ magnetism. In agreement with x-ray diffraction and magnetization data, the resistivity of Yb_2In is rather featureless and typical of a metal. Establishing Yb_2In as a nonmagnetic isostructural reference for Eu_2In allows one to use its heat capacity to revisit that of the latter, and get experimental insights into the exceptional magnetocaloric effect of the compound with Eu. In particular, we show that a third of the total magnetic entropy ($S_m \approx 35.6\,J\,mol^{-1}\,K^{-1}$ at $T = 100\,K$) is concentrated in a 3 K temperature window around the T_C of Eu_2In. Starting from the ferromagnetic compound Eu_2In [$T_C = 55.2(5)$ K], we show that Yb substitutions in $Eu_{2-x}Yb_xIn$ lead to a decrease in both the Curie temperature [$T_C = 41(2)$ and 32(2) K for $x = 0.25$ and 0.5] and magnetic saturation, while weakening the first-order character of the transition as x increases. A significant isothermal entropy change of $5.1(4)\,J\,mol^{-1}\,K^{-1}$ for $\Delta B = 2\,T$ is found at 44 K in $Eu_{1.75}Yb_{0.25}In$, demonstrating that the giant magnetocaloric effect of Eu_2In can be tuned to lower temperatures by Yb substitutions.

DOI: 10.1103/PhysRevMaterials.4.104402

I. INTRODUCTION

Due to localized *4f* electrons with large moments and strong spin-orbit coupling, rare-earth (*RE*) intermetallics represent an interesting playground for intriguing magnetic phenomena, which explains why these alloys remain a fascinating subject for materials scientists and condensed-matter physicists. Despite the apparent simplicity of their binary 2:1 nominal compositions and an abundance of interesting physical phenomena, the properties of RE_2In intermetallics are not yet fully explored nor understood. The crystal structures and magnetic properties of RE_2In with trivalent *RE*s have been subjects of several studies [1–3], in particular for Gd_2In, which shows a field-induced metamagnetic transition with significant magnetoresistance and magnetocaloric effect [4–8]. On the other hand, the physical properties of RE_2In with potentially divalent rare-earth elements, such as Eu and Yb, are comparatively unknown, albeit being probably the most interesting owing to their additional valence degrees of freedom. For example, ferromagnetism in Eu_2In was discovered only recently [9], even though its crystal structure (orthorhombic Co_2Si type) was reported nearly three decades ago [10]. The ferromagnetic transition at $T_C = 55.2(5)$ K in Eu_2In is worth investigating in detail because it is associated with a large latent heat corresponding in the Ehrenfest classification to a first-order transition [11], i.e., a first-order magnetic transition (FOMT), but the thermal hysteresis is very small (less than 0.1 K), making Eu_2In one of the rare examples of nearly ideal FOMT. In addition, application of an external magnetic field near T_C in adiabatic or isothermal conditions leads to a large change in temperature or entropy, respectively, so that Eu_2In can be regarded as a giant magnetocaloric effect material [9].

The case of Yb-containing RE_2In is also particularly interesting because Yb can be either trivalent (behaving like a lanthanide metal) or divalent (behaving like an alkaline-earth metal) in intermetallics. In a few known examples, it may even exhibit mixed valence, or valence fluctuations as a function of the temperature in alloys of Yb and *p*-block elements, leading

*hyibole@imnu.edu.cn

to unconventional properties such as Kondo effect, negative thermal expansion, Lifshitz transition, etc. [12,13]. The synthesis and orthorhombic $PbCl_2$-type crystal structure of binary Yb_2In have already been reported [14]. Nevertheless, to the best of our knowledge, no comprehensive study of its physical properties is available.

In this work, the case of Yb containing RE_2In alloys and their comparison with Eu_2In is investigated. First, the similarity in structure and bonding between Yb_2In and Eu_2In is established in Sec. III A. Then, physical properties of Yb_2In are explored in details in Sec. III B in order to demonstrate the divalent nature of Yb in Yb_2In, so that this latter can be used as a nonmagnetic isostructural reference to revisit some physical properties of Eu_2In, including a more detailed analysis of the heat capacity data originally reported in Ref. [9]. Finally, in Sec. III C an exploratory study of the structure and magnetic properties of intermediate $Eu_{2-x}Yb_xIn$ alloys is carried out with the goal of finding pathways to tune the giant magnetocaloric effect of Eu_2In over an extended temperature range.

II. EXPERIMENTAL DETAILS

Seven $Eu_{2-x}Yb_xIn$ alloys were prepared using a sealed tantalum ampule method to avoid Eu or Yb evaporation. The elemental rare-earth starting materials were obtained from the Baotou research institute of rare earths (high-purity grade given as $\geqslant$99.9 wt.%) and In ingot from Alfa Aesar ($\geqslant$99.99%). The starting materials were weighed in stoichiometric proportions in a purified Argon MBraun glovebox (total mass approximately 5 g) and loaded into Ta ampules of 1 cm diameter and 4 cm length. The Ta ampules were pumped at high vacuum (10^{-5} mbar), then back-filled with partial Ar atmosphere ($\sim$500 mbar), arc welded, and finally sealed in quartz tube to prevent Ta oxidation at high temperatures. The resulting ampules were heated to 1000 °C and held at this temperature for 6 h three times, while being flipped over each time for better mixing of the components. After the third heating, final annealing was performed at 700 °C for 48 h. The resulting alloys have a gray, relatively shiny, metallic appearance. Exposure to moist air leads to decomposition. Even though chemical reactivity of Yb-containing samples is significantly lower than Eu_2In, all sample manipulations, except sample mounting for heat capacity measurements, were carried out in the glovebox.

X-ray-powder-diffraction experiments were performed on a Panalytical Empyrean x-ray diffractometer using Cu-Kα radiation. Temperature-dependent x-ray-powder-diffraction measurements in the range from 100 to 375 K were carried out using an Anton Paar TTK600 low-temperature chamber. The samples were ground into powders in a glovebox, and then mixed with petroleum jelly to limit decomposition in air. The presence of petroleum jelly produces a broad amorphous contribution centered on $2\theta = 18^\circ$ and two weak peaks at 21.3° and 23.7°. Mixing with petroleum jelly prevents sample decomposition during a typical 2-h scan, but longer exposures to outside air show phase changes in the diffractograms, which imposes limitations on the quality of the patterns. The FULLPROF software was used to perform Rietveld refinements [15].

Physical property measurements were carried out in Quantum Design Versalab (50–400 K) and PPMS (2–400 K) systems. Vibrating sample magnetometer option was employed for magnetic measurements. The magnetic background of the sample holder (brass half-tube sample holder with the sample fixations) was recorded in 1 T (from -9.10^{-6} at 50 K to $+7.10^{-6}$ emu at 300 K) and subtracted for magnetic measurements of Yb_2In. Due to the low magnetization of Yb_2In (raw signals in the range -2.10^{-4} to -9.10^{-5} emu), the magnetization measurement for this sample appears relatively noisy; in addition, steplike artifacts due to periodic recentering of the sample ("touchdown") are observed at certain temperatures. Electrical resistivity (ρ) measurements were carried out on bulk bars of approximately $10 \times 2 \times 3\,mm^3$ using an electrical transport option of PPMS; the contacts were attached using silver epoxy. $\rho(T)$ curves were measured on heating in a sweep mode at 1 K/min. A semiadiabatic heat capacity option with standard "2τ" analysis is used for Yb_2In. The heat capacity data for Eu_2In originate from a former work using a similar measurement setup [9].

III. RESULTS AND DISCUSSION

A. Reassessment of Yb_2In structure including its temperature dependence

Figure 1(a) shows the powder x-ray-diffraction (XRD) patterns of Eu_2In and Yb_2In. Both can be indexed in the orthorhombic Co_2Si-type structure. For the Eu-containing samples a secondary Eu_8In_3 phase is detected; its fraction is limited for $x = 0$ [$\sim$ 4(1) wt.%]. For Yb_2In, a nearly negligible [$\sim$2(1) wt.%] of the unreacted In phase can be detected. The main difference noticeable on the powder XRD from Eu_2In to Yb_2In is a substantial shift of all Bragg reflections toward higher angles. Yb_2In is found to present a significantly smaller cell volume than Eu_2In, which is expected considering that Eu^{2+} has the largest atomic radius among all lanthanides. The refined lattice parameters for Yb_2In are $a = 7.093(1)$ Å, $b = 5.3296(7)$ Å, and $c = 9.884(2)$ Å, which are in reasonable agreement with the earlier report [14]. While the crystal structure of Yb_2In was originally described as a $PbCl_2$-type compound, the ratios of the lattice parameters $b/a = 0.751$ and $a/c = 0.717$, as well as the coordination of the In atom with 10 nearest-neighbor Yb atoms, are more typical of the closely related Co_2Si-type structure [16]. When considering the cell volume of hexagonal (trivalent *RE*s) or orthorhombic (divalent Eu and Yb) RE_2In alloys ($V_{ortho} = 2V_{hexa}$) as a function of the atomic number of the rare-earth, Eu_2In and Yb_2In clearly stand out [Fig. 1(b)]. The difference between the experimentally observed unit-cell volume of Yb_2In [$V_{ortho} = 373.7(1)$ Å^3] and that extrapolated from the trivalentlike RE_2In line is approximately $\sim$15.5%. This forms a first indication of a predominantly divalent Yb^{2+} state in Yb_2In, as this difference is as large as the difference between their effective ionic radii (Yb^{2+}:1.14 Å, Yb^{3+}:0.985 Å) [17] and even slightly larger than the expected difference between the metallic radii of divalent and trivalent ytterbium (Yb^{2+}:1.94 Å, Yb^{3+}:1.74 Å) [18].

From similar geometric arguments, the temperature dependence of the unit cell can also provide additional insight into

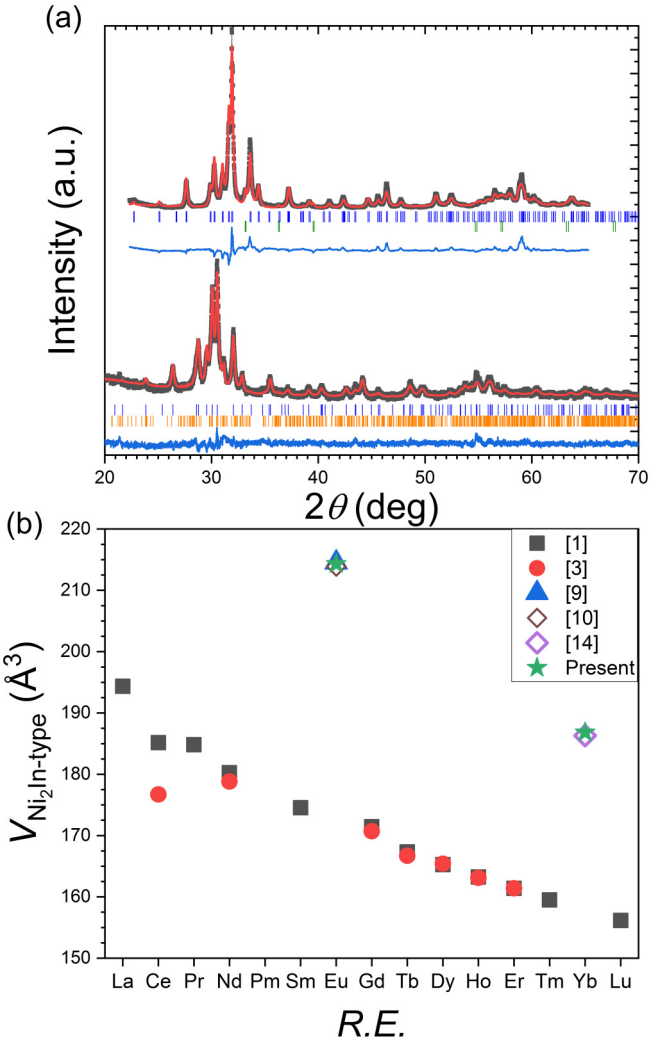

FIG. 1. (a) Room-temperature XRD patterns for Yb_2In (top) and Eu_2In (bottom), experimental data (symbols), refined intensity (lines), and their differences (lower curves). The tick marks indicate the Bragg peak positions for Co_2Si-type crystal structure (top row of tick marks) and for In or Eu_8In_3 secondary phases (bottom row of tick marks) for Yb_2In and Eu_2In, respectively. (b) Comparison of the unit-cell volumes within the RE_2In family (cell volumes of Eu_2In and Yb_2In are one half of the volumes of the corresponding orthorhombic cell).

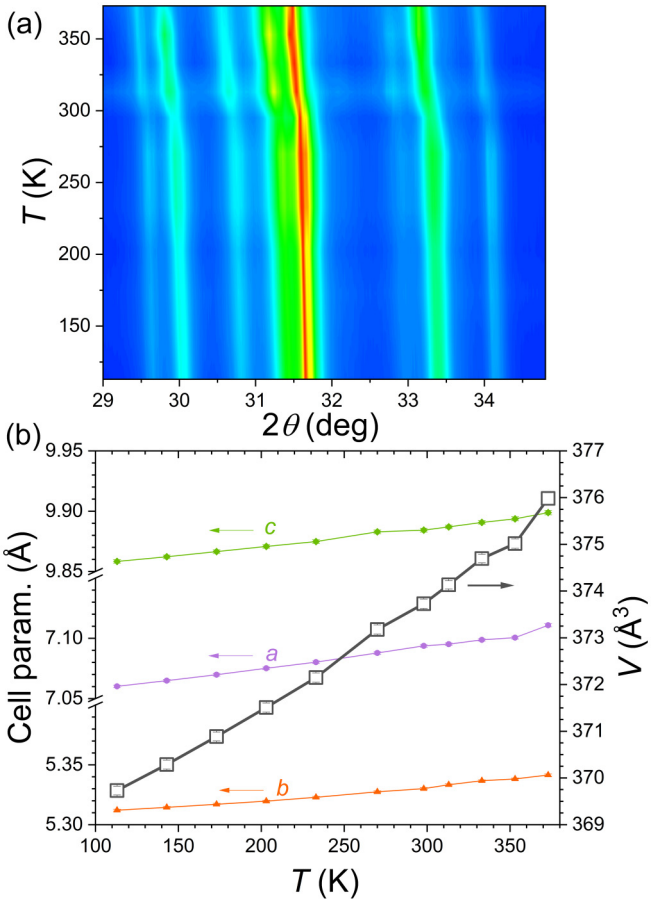

FIG. 2. Powder XRD as a function of the temperature in Yb_2In: contour map of the XRD patterns in the temperature range between 100 and 375 K plotted for clarity around the most intense Bragg reflections, from 29 to 35° (2θ) (a), and temperature dependences of the lattice parameters (left-hand scale) and the unit-cell volume (right-hand scale) (b). On the contour map, some fluctuations in intensity are noticeable around 300 K due to the melting of petroleum jelly.

the stability of the divalent Yb state in Yb_2In, in particular as thermally induced valence fluctuations in Yb intermetallics can result in unconventional thermal expansion [12]. Figure 2 presents the contour plot of the diffraction patterns of Yb_2In as a function of the temperature around the most intense Bragg peak (013) at $2\theta \approx 31.7°$ and the temperature dependence of the unit-cell parameters and volume. Qualitatively, no new Bragg peaks appear/existing peaks disappear in the studied temperature range and there are no obvious discontinuities. There is a progressive shift of all Bragg reflections toward lower angles with raising the temperature, indicating that Yb_2In experiences a progressive cell-volume expansion on heating. The temperature dependence of all lattice parameters is nearly featureless with a similar expansion in all directions (only very slightly anisotropic). As a result, the cell volume increases monotonically [thermal expansion coefficient $(1/V)(dV/dT) \approx +6 \times 10^{-5}\,\mathrm{K}^{-1}$] without any sign of negative thermal expansion, which suggests a stable Yb^{2+} configuration over the temperature range 100–375 K. In the isostructural Eu_2In, a stable divalent state for the rare earth was also observed over a large temperature range and confirmed by x-ray absorption and Mössbauer spectroscopies [9,19].

B. "Nonmagnetic" Yb_2In as an isostructural reference for revisiting the heat capacity of Eu_2In

In contrast to Eu_2In [9] or $Eu_{2-x}Yb_xIn$ pseudobinaries (presented in Sec. III C), the magnetic susceptibility of Yb_2In is very small and negative (see Fig. 3), in support of a nonmagnetic Yb divalent state with the total angular momentum quantum number $J = 0$. But this $\chi(T)$ curve presents an upturn at low temperatures, which also suggests a minor paramagnetic contribution indicative of the likely presence of parasitic Yb^{3+} [20]. Accordingly, we fit our data as the sum of temperature-independent susceptibility, χ_0,

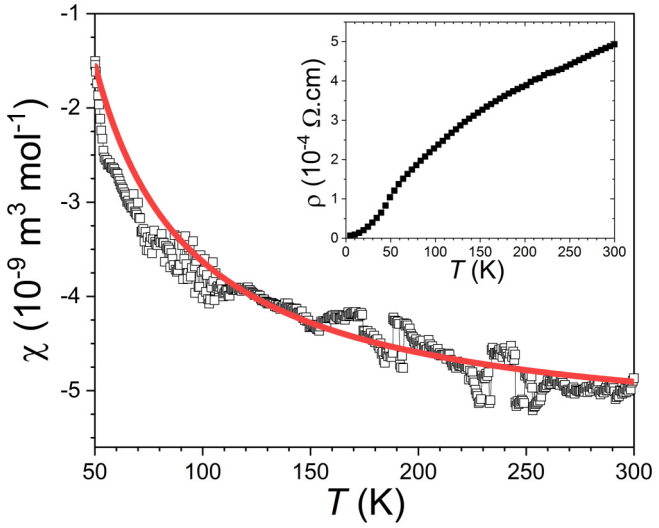

FIG. 3. Magnetic susceptibility of Yb_2In recorded in $B = 1$, T. Solid line represents Curie-Weiss fit assuming a small fraction of Yb^{3+} is present (see text for details). In inset, temperature dependence of the resistivity of Yb_2In measured in $B = 0$.

representative for divalent Yb^{2+} and the Curie-Weiss term accounting for Yb^{3+} fraction: $\chi(T) = (1-n)\chi_0 + nC_{Yb3+}/(T-\theta_W)$; where n represents the Yb^{3+} fraction, the Curie constant $C_{Yb}^{3+} = [g^2J(J+1)\mu_B{}^2]/(3k_B)$ is calculated using the Landé spectroscopic factor $g = 8/7$ and the total angular momentum $J = 7/2$ of free Yb^{3+} ion corresponding to a theoretical effective magnetic moment of $4.54\,\mu_B$ per Yb^{3+}, and assuming the absence of crystal-field effect on Yb^{3+} above 50 K. The magnetization presented in Fig. 3 could be fitted using $\chi_0 = -5 \times 10^{-9}\,m^3\,mol(Yb_2In)^{-1}$ and $n = 0.3\%$, which suggests an extremely small Yb^{3+} content. Assuming that Yb^{3+} originates from antiferromagnetic Yb_2O_3 contamination [20,21], a slightly negative Weiss temperature ($\theta_W = -3$ K) is included, but its influence on the fit remains limited. A further indication that Yb^{3+} originates from minor impurity phases resulting from the sample oxidation is its increasing fraction when remeasuring periodically the same batch of Yb_2In (n increased from ~0.3 to ~2% over a period of 9 months even when held in the glovebox; see Supplemental Material [22]). We note that the small negative χ_0 magnetic susceptibility value in Yb_2In is close to that observed in other intermetallics containing Yb^{2+} [20,23]. This strongly supports the divalent nature of ytterbium in Yb_2In, the absence of significant changes in Yb valence as a function of temperature, and suggests that Yb_2In is a diamagnetic compound.

The electrical resistivity (ρ) of Yb_2In in zero magnetic field is shown in the inset of Fig. 3. The temperature dependence of the resistivity of Yb_2In is metallic and rather featureless, in accordance with the $M(T)$ and XRD vs T data. At high temperatures, it shows almost linear temperature dependence above 150 K, where the electrical resistivity is dominated by electron-phonon scattering with the phonon concentration proportional to the temperature [24], providing a rough estimate of the Debye temperature from resistivity data. This relatively low Debye temperature assessed from the resistivity measurements [150(15) K] is in agreement with that obtained

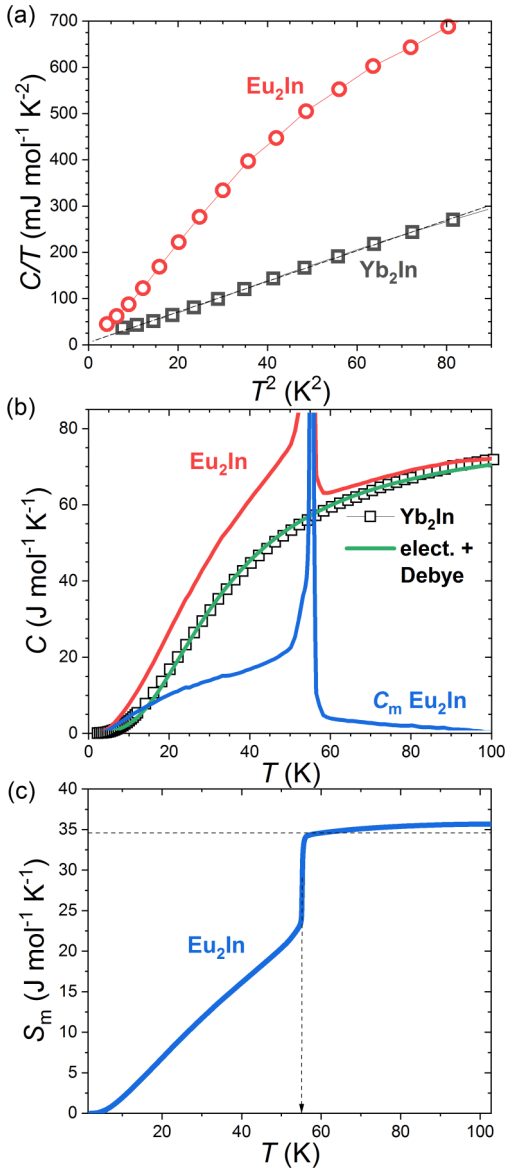

FIG. 4. Heat capacity in zero magnetic field of Eu_2In and Yb_2In. (a) low temperature C/T vs T^2; (b) calculation of the magnetic contribution for Eu_2In using the experimentally obtained Yb_2In heat capacity (open squares); (c) Temperature dependence of the magnetic entropy in Eu_2In. The horizontal dashed line represents the magnetic entropy in the high-temperature limit of the localized Brillouin model and the vertical arrow marks out $T_C = 55.2(5)$ K of Eu_2In.

hereafter from heat capacity data [137(5) K, see below]. At lower temperatures ($T < 50$ K), the $\rho(T)$ curve shows the development of a curvature recalling the T^n-like dependence anticipated for metals [24]. This temperature evolution is in marked contrast with the discontinuity in resistivity observed at T_C of Eu_2In [9] or anomalies observed in other RE_2In materials at their magnetic ordering transitions [4,25,26].

Figure 4 presents the heat capacity of Yb_2In along with the previously reported Eu_2In data [9]. The temperature dependence of the heat capacity in Yb_2In does not reveal any peculiar anomalies, which is fully consistent with the structural and physical properties presented hereabove. On the

other hand, Eu_2In presents an exceptionally sharp and high heat capacity peak at its Curie temperature $T_C = 55.2(5)$ K [9]. In the low-temperature range [$2 < T < 10$ K, Fig. 4(a)], if the nuclear contribution is neglected, the contributions to the heat capacity usually considered are [27]: a phononic term C_{lat} related to lattice vibrations modeled in first approximation as a βT^3 contribution; an electronic term of the form γT that is related to free charge carriers; and a magnetic contribution C_{mag}. The C/T vs T^2 evolution for Yb_2In turns out to be nearly linear below 10 K, while it remains nonlinear and shows larger values for Eu_2In [Fig. 4(a)]. This is consistent with the absence of magnetic contribution in the former, while in the latter the magnetic contribution is significant below 10 K. In the case of Yb_2In, we can estimate the electronic term $\gamma \approx 5(1)$ mJ mol^{-1} K^{-2} and cubic lattice term $\beta \approx 3.3(2)$ mJ mol^{-1} K^{-4}, allowing in turn to estimate the Debye temperature in the low-temperature limit as $\theta_{D-LT} = (12\pi^4 nR/5\beta)^{1/3} \approx 120(3)$ K, with the molar gas constant $R = 8.314$ J mol^{-1} K^{-1} and $n = 3$ atoms f.u.$^{-1}$. Such a modest Debye temperature is in line with the values reported in closely related materials such as in orthorhombic RE_2Al compounds ($\theta_{D-LT} = 180$, 180, and 221 K for RE = Nd, Tb, and Gd, respectivly) [28] or in hexagonal RE_2In compounds where heat capacities close to the Dulong and Petit value are reached around 150 K [6,29,30].

Over a broader temperature range [Fig. 4(b)], heat capacity of Yb_2In was modeled considering the complete expression of the Debye heat capacity and an electronic term $C = \gamma T + 9nR(\frac{T}{\theta_D})^3 \int_0^{\theta_D/T} \frac{x^4 e^x}{(e^x-1)^2} dx$, leading to $\theta_D = 137(5)$ K. The reasonable agreement that can be obtained between the modeled and experimental heat capacity data is consistent with the fact that no magnetic contribution is expected for the divalent ytterbium in Yb_2In.

The temperature dependences of magnetic specific heat [C_m, Fig. 4(b)] and magnetic entropy $S_m = \int_0^T \frac{C_m}{T} dT$ of Eu_2In [Fig. 4(c)] were obtained by assuming that the lattice and electronic contributions to heat capacity are similar in Eu_2In and Yb_2In and subtracting the experimental $C(T)$ data of Yb_2In from the experimental $C(T)$ data of Eu_2In measured earlier. It should be recalled that "traditional" nonmagnetic reference compounds such as La_2In could not be employed here because RE_2In with trivalent-like RE crystallize in a different crystal structure. The accuracy of this approach relies on the assumption of identical lattice and electronic contributions in Eu_2In and Yb_2In. This approximation turns out to be sound for several reasons. For the lattice contribution, if a Debye model of the lattice heat capacity is considered, finding C_{lat} for Eu_2In reduces to deriving the Debye temperature of the magnetic sample $\theta_D(Eu_2In)$ from that of the nonmagnetic isostructural reference $\theta_D(Yb_2In)$. These Debye temperatures are affected by the atomic mass difference between Eu and Yb, which is usually corrected as $\theta_D(Eu_2In)/\theta_D(Yb_2In) = [M_{mol}(Eu_2In)/M_{mol}(Yb_2In)]^{-1/2}$ where M_{mol} represent the molar masses. In addition, the difference in molar volume V_{mol} between Eu_2In and Yb_2In should also be taken into account [27], leading at the end to an evolution of the Debye temperatures that is anticipated to vary as $\theta_D \propto M_{mol}^{-1/2} V_{mol}^{-1/3}$. It follows that the correction factor r to rescale the lattice contributions of Eu_2In with respect to that of Yb_2In is close to unity and can be disregarded:

$$r = \frac{\theta_D(Eu_2In)}{\theta_D(Yb_2In)} = \frac{V_{mol}^{1/3}(Yb_2In)\, M_{mol}^{1/2}(Yb_2In)}{V_{mol}^{1/3}(Eu_2In)\, M_{mol}^{1/2}(Eu_2In)} \approx 1.003.$$

For the electronic contribution, there is *a priori* no reason to consider the electronic γ terms to be similar in Eu_2In and Yb_2In. We however note that: (i) electronic contribution influence is limited as the electronic term represents less than a percent of the total heat capacity near 50 K; (ii) these two materials exhibit similar electrical resistivities at room temperature, and (iii) despite its nonlinearity, the C/T vs T^2 dependence of Eu_2In tends to extrapolate toward a similar intercept as Yb_2In. In other respect, the γ term for Eu_2In estimated from the electronic density of states at the Fermi level [$N(E_F)$] obtained by first-principles calculations ($N(E_F) \approx 1.9$ states eV^{-1} f.u.$^{-1}$ [9]) amounts to $\gamma = [\pi^2 k_B R N(E_F)]/3 \approx 4.5$ mJ mol^{-1} K^{-2}, i.e., very close to that found experimentally here for Yb_2In [$\approx$5(1) mJ mol^{-1} K^{-2}].

The subtraction of the heat capacity of Yb_2In from the heat capacity of Eu_2In leads to the magnetic specific heat (C_m) of Eu_2In [Fig. 4(b)]. A magnetic contribution to heat capacity grows rapidly from low temperature up to ~20 K, where it forms a broad hump (even more salient on a C_{mag}/T vs T curve). We note that such a feature in $C_m(T)$ is often observed around $T \approx T_C/3$ in Eu-based intermetallics [31,32]. More unusual is the extreme sharpness of the peak on $C_m(T)$ marking the first-order ferromagnetic transition of Eu_2In. Further, one observes that C_m is nonzero above T_C and becomes negligible only above ~95 K. This nonzero magnetic contribution up to ~1.7 T_C may reflect the presence of dynamic short-range ferromagnetic correlations above T_C. The temperature up to which sizable C_m persists (~95 K) corresponds to the temperature where a deviation from the Curie-Weiss law was observed in DC magnetic measurements and where a gradual increase in χ' or χ'' upon cooling was detected in AC susceptibility measurements [9]. A more detailed study of this anomaly emerging from 95 K would, however, be required as its magnitude has been found to vary from sample to sample.

The total magnetic entropy of Eu_2In, $S_m \approx 35.6$ J mol(Eu$_2$In)$^{-1}$ K^{-1} at $T = 100$ K [see Fig. 4(c)] is slightly larger than—yet still fully compatible with—that expected in the high-temperature limit of the localized Brillouin model, i.e., $R\ln(2J+1) = 34.6$ J mol(Eu$_2$In)$^{-1}$ K^{-1} with $J = 7/2$ the total angular momentum of Eu^{2+}.

Even though a small excess in the experimental magnetic entropy may be ascribed to uncertainties in the subtraction of lattice and electronic contributions, it may also originate from the finite magnetic moments developing on polarized Eu-d and In-p states. Nonzero itinerant moments are predicted by density-functional theory band-structure calculations and are in line with a saturation magnetization [$M_{sat} \approx 14.4 \mu_B$/f.u.(Eu$_2$In)], which is slightly larger than that expected for Eu^{2+} (14 μ_B/f.u.) [9,33]. Besides, a possible change in the structural contribution to the heat capacity at the ferromagnetic transition was neglected. At T_C, the entropy change associated with the elastic energy of the volume change could be estimated as $\Delta S_{elastic} = (B(\Delta V/V)^2)/(2T_C)$ [34], where $\Delta V/V \approx 0.1\%$ is the relative volume change at the transition and B the bulk elastic

modulus. The estimate of this contribution is very crude due to the unavailability of appropriate B values, nevertheless using $B \approx 38$ GPa of the closely related Gd_2In [35], one gets $\Delta S_{elastic} \approx +0.02\,J\,mol^{-1}\,K^{-1}$, a value so small that it can safely be neglected in comparison to the large total entropy change of the transition. Over a broader temperature range, the change in lattice contribution might be anticipated to be linked to that of the Debye temperature, $\Delta\theta_D/\theta_D = \Gamma\Delta V/V$ where Γ is the Grüneisen parameter [34]. The change in Debye temperature being proportional to the very limited cell-volume change at T_C, this lattice contribution evolution can also be neglected in first approximation.

Finally, $S_m(T)$ of Eu_2In is primarily remarkable for its temperature evolution, with the ΔS_m discontinuity at T_C representing $\sim 12\,J\,mol^{-1}\,K^{-1}$ in a 3 K temperature window, i.e., a concentration of the 1/3 of the total magnetic entropy in a narrow temperature interval. Furthermore, the S_m discontinuity alone in Eu_2In is much larger than the $6\,J\,mol^{-1}\,K^{-1}$ magnetic entropy found in the closely related Gd_2In intermetallic [5]. Therefore, the present data provide direct experimental support to the initially proposed idea that strong change in S_m in the narrow temperature interval is at the origin of the exceptionally large magnetocaloric effect in Eu_2In. This large magnetic entropy discontinuity can be reversibly shifted above T_C by a magnetic field change as small as 1 T without incurring any energy losses [9].

C. Evolution of structure, magnetism, and magnetocaloric effect in $Eu_{2-x}Yb_xIn$ pseudobinaries

To investigate the effect of nonmagnetic Yb substitutions in Eu_2In, a series of $Eu_{2-x}Yb_xIn$ pseudobinary alloys was prepared and investigated. The XRD patterns of all alloys could be refined using the same Co_2Si-type structure as Eu_2In and Yb_2In, suggesting that they form a continuous solid solution. Figure 5 presents the evolution of the cell volume in the series with Yb substitution. The cell-volume reduction in $Eu_{2-x}Yb_xIn$ alloys shows negative deviation from linearity around $x = 0.75$. Deviations from Vegard's law are known to occur when one rare-earth element is substituted for another [36], yet this deviation is also influenced by the formation of Eu_8In_3 secondary phases in $Eu_{2-x}Yb_xIn$ samples with $0.5 < x < 2$ (roughly estimated up to 11 wt.%; see Supplemental Material, section S2 for additional details [22]).

Figure 6 presents the magnetic properties of $Eu_{2-x}Yb_xIn$ alloys. A clear first-order ferromagnetic transition is observed near $T_C \approx 55.2(5)$ K of Eu_2In. With the increase in Yb concentration, the ferromagnetic ordering transition temperature shifts to lower temperatures and progressively broadens up to $x \sim 0.5$. The transition temperatures defined as dM/dT minima of $M(T)$ recorded in $B = 0.1$ T are presented in the inset of Fig. 6(a). From $x \geqslant 0.75$, the magnetization in $B = 1$ T drops even more rapidly, suggesting disappearance of the long-range ferromagnetic order (see Supplemental Material, section S3 [22]). An inflection point can nevertheless be observed on $M(T)$ curves at low temperatures for $x = 0.75$ and $x = 1$ [referred to as T^* in Fig. 6(a)], unlikely to originate from the Eu_8In_3 secondary phase as it is composition dependent, which may indicate the development of short-range magnetic order. For $x \geqslant 0.25$, $M(T)$ curves [or $M(B)$ curves] show a

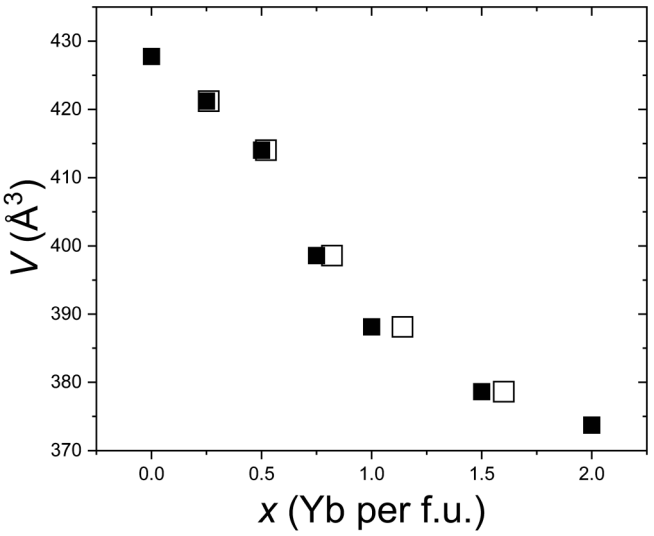

FIG. 5. Cell volume of $Eu_{2-x}Yb_xIn$ calculated from the powder XRD data indexed in the Co_2Si-type structure (closed symbols are for the nominal values of x, and open symbols are for the values of x corrected for the presence of Eu_8In_3 impurities in concentrations estimated from the Rietveld analysis of the data).

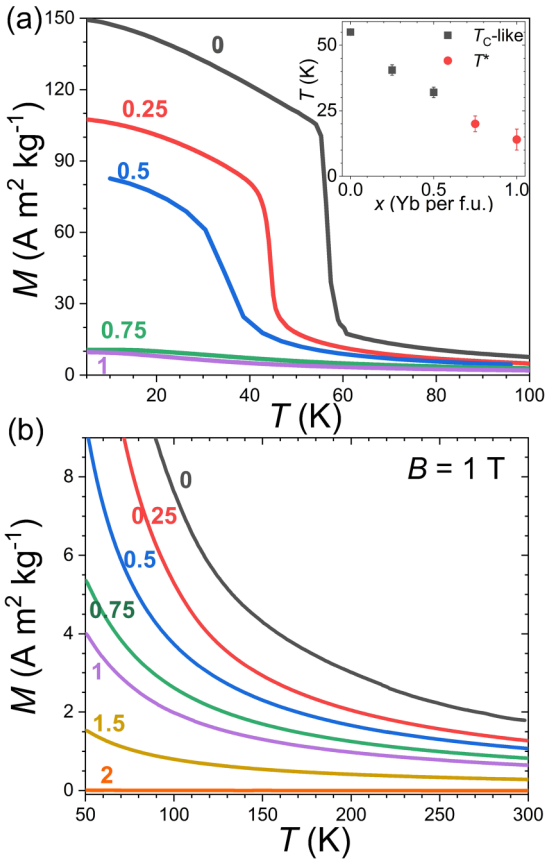

FIG. 6. Magnetic properties of $Eu_{2-x}Yb_xIn$ alloys (the nominal x values are indicated along each magnetization curve). (a) Low-temperature $M(T)$ curves measured upon heating in $B = 1$ T. The inset shows transition temperatures (taken in $B = 0.1$ T) plotted as a function of Yb content. (b) $M(T)$ data obtained upon heating in $B = 1$ T in the temperature range between 50 and 300 K.

progressive decrease in magnetization with the increase in Yb. In the temperature range 50–300 K, χ^{-1}(T) curves are linear (except for Yb_2In) and could be fitted by a Curie-Weiss law. The Weiss temperatures and effective moments progressively decrease with Yb substitutions (see Supplemental Material, section S3 [22]). The present magnetization data are thus in line with the evolution expected for a gradual substitution of magnetic Eu^{2+} by nonmagnetic Yb^{2+}. A more detailed analysis of the magnetic properties of intermediate $Eu_{2-x}Yb_xIn$ alloys from our data is hardly possible at present due to non-negligible secondary phase contamination in $0.5 < x < 2$ samples.

To gain further insight into the effect of limited Yb substitution on the ferromagnetic transition of Eu_2In and its magnetocaloric effect, a set of isothermal $M_T(B)$ magnetization curves was recorded for $x = 0.25$, see Fig. 7. First, the magnetization at 5 K does not fully saturate, and it reaches only 120 $Am^2\,kg^{-1}$ (~9.3 μ_B/f.u.) at 7 T, which turns out to be significantly smaller than the 12.6 μ_B/f.u. value expected for this composition when using saturation magnetization of Eu_2In [9]. At higher temperatures, field-induced magnetization jumps are observed near the Curie temperature revealing a first-order magnetic transition. Similar to the case of Eu_2In [9], the associated field hysteresis is small (~0.1 T and less) and the material fully returns to its original paramagnetic state upon demagnetization. However, in contrast to Eu_2In, the amplitude of the magnetization jumps is more limited and they broaden more rapidly with the increase in temperature, suggesting a weaker first-order character.

The magnetocaloric effect of the $x = 0.25$ sample was calculated by applying the Maxwell equation to the $M(B)$ data [37]. The corresponding isothermal entropy changes are presented for different magnetic fields in Figs. 7(b) and 7(c). The maxima of the $-\Delta S(T)$ curves swiftly increase up to 2 T, then they show a more monotonous increase. This initial regime corresponds to the rapidly increasing contribution from the latent heat of the paramagnetic to ferromagnetic first-order transition, whereas the slower high-field evolution represents the conventional caloric response of the field-induced ferromagnetic phase. These two contributions are particularly noticeable on the field evolution of the $-\Delta S$ for a temperature fixed at T slightly higher than the T_C in $B = 0.1$ T (in practice at the transition temperature in $B = 1$ T), see Fig. 7(c). The entropy anomaly due to the first-order contribution presents an S-like discontinuous shape up to 2 T and amounts to ~5 $J\,mol^{-1}\,K^{-1}$. Once the latent heat is fully released by the increasing field, one is left with a more monotonous change of $-\Delta S$. This result is supported by the mean-field modeling of Eu_2In compound, which suggests a qualitative transition from a first into a second-order behavior in Eu_2In at ~2.5 T [38]. The entropy anomaly at the first-order transition of $Eu_{1.75}Yb_{0.25}In$ is half that observed in Eu_2In (~12 $J\,mol^{-1}\,K^{-1}$), resulting in much smaller magnetocaloric effect. At higher magnetic fields (3–7 T), the $-\Delta S$ values progressively increase (up to 8.2 $J\,mol^{-1}\,K^{-1}$ in 7 T), but remain modest as the magnetization is relatively limited compared to Eu_2In. In addition, the $-\Delta S(T)$ curve profile does not correspond to the expected tablelike shape for an FOMT [39]. Yet, the high temperature–high-field side is considerably broader than the low-T part, which is different from the second-order

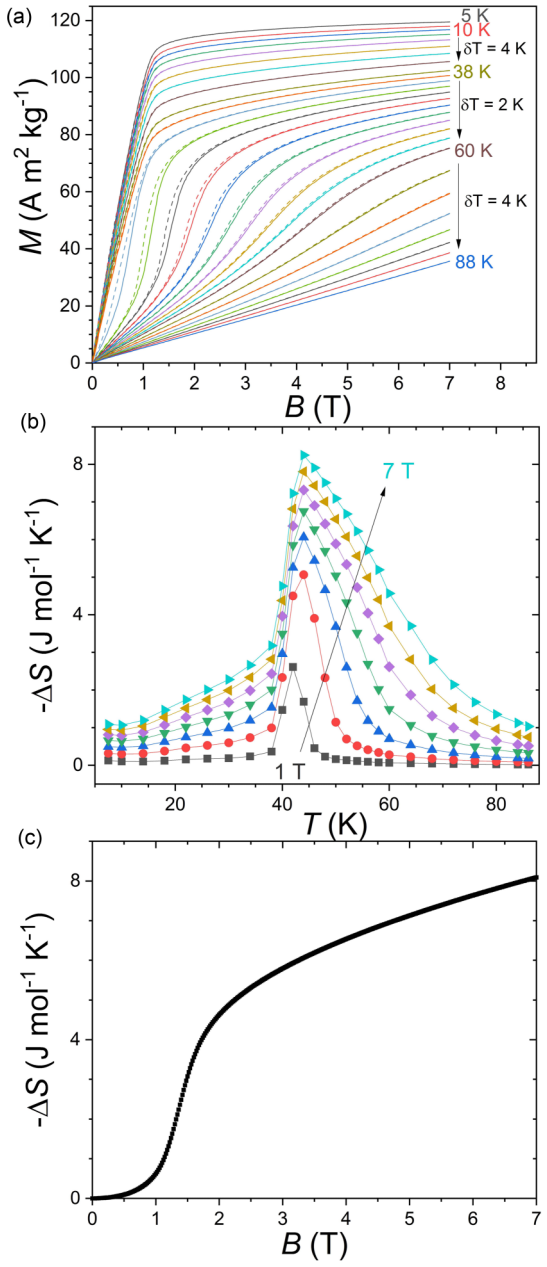

FIG. 7. Magnetization and magnetocaloric effect of $Eu_{1.75}Yb_{0.25}In$. (a) Magnetization (solid lines) and demagnetization (dashed lines) curves recorded for different temperatures. (b) Temperature dependence of the opposite of the isothermal entropy change for different applied magnetic fields from 1 to 7 T in 1-T increments. (c) Field dependence of the magnetocaloric effect at 45 K.

transitions, where $-\Delta S(T)$ is mostly symmetric. This asymmetry was present in Eu_2In [9], but is exacerbated upon Yb substitution. It primarily originates from the broadening of the FOMT at high field and the progressive field-induced evolution toward the crossing of a critical point where the first order turns into a second-order transition. The weaker the FOMT in zero field, the more pronounced this phenomenon appears to be. Even though materials considered in this paper are unlikely to find practical use due to the high costs and

criticality of the constituting elements, they represent an interesting example of tunability: Yb for Eu substitutions can be used to tune the magnetocaloric effect of Eu_2In toward lower temperatures (at least down to 30 K), but at the expense of its magnitude. This decrease in magnetocaloric effect upon Yb substitution originates from both the decrease in magnetization and weakening of the FOMT.

IV. CONCLUSIONS

Due to Yb_2In crystallizing in the same orthorhombic Co_2Si-type structure as Eu_2In, the $Eu_{2-x}Yb_xIn$ compounds form a continuous solid solution with a negative deviation from Vegard's law. Based on the experimentally determined lattice parameters, Yb is expected to be in a divalent Yb^{2+} state, which is in line with a $J = 0$ configuration observed from magnetization measurements. Yb for Eu substitutions in Eu_2In are found to decrease the ordering temperature and magnetic saturation, and broaden the first-order ferromagnetic transition when compared with Eu_2In. From a magnetocaloric point of view, Yb substitutions ($x \leqslant 0.5$) in Eu_2In may be used to decrease the temperature range where a giant magnetocaloric effect is observed, but the effect is substantially weakened. The electrical resistivity of Yb_2In is metallic and rather featureless, in line with the anomaly-free temperature dependence of XRD and magnetization data. The heat capacity measurements for Yb_2In both confirm absence of anomalies in Yb_2In and allow one to use Yb_2In as an isostructural reference to obtain and analyze magnetic contribution to heat capacity of Eu_2In. The magnetic entropy of Eu_2In is experimentally obtained and shows an unusual distribution with 1/3 of the available S_m concentrated within less than 3 K around the magnetic ordering transition, which is primarily responsible for the exceptional magnetocaloric effect of Eu_2In.

ACKNOWLEDGMENTS

The work is supported by the Inner Mongolia Normal University (Grants No. 2018YJRC002 and No. 2018YJRC003), the program for young talents of science and technology in universities of Inner Mongolia Autonomous Region (Grant No. NJYT-20-A17) and the Natural Science Foundation of China (Grants No. 51850410514, No. 51961033, and No. 11904188). Work at Ames Laboratory was supported by the Division of Materials Science and Engineering, Basic Energy Sciences, Office of Science of US Department of Energy (DOE). Ames Laboratory is operated for the US DOE by Iowa State University of Science and Technology under Contract No. DE-AC02-07CH11358.

[1] A. Palenzona, The crystal structure and lattice constants of RE_2In and some RE_5In_3 compounds, J. Less-Common Metals **16**, 379 (1968).

[2] H. Gamari-Seale and T. Anagnostopoulos, Magnetic characteristics of rare-earth indium R_2In (R = Y, Nd, Sm, Gd, Tb, Dy, Ho, Er, and Tm) intermetallic compounds, J. Appl. Phys. **50**, 434 (1979).

[3] W. Baela and A. Szytuła, Crystal structure and magnetic properties of RE_2In compounds, J. Less-Common Metals **138**, 123 (1988).

[4] S. P. McAlister, Magnetic and electrical properties of Gd_2In, J. Phys. F: Met. Phys. **14**, 2167 (1984).

[5] C. S. Jee, C. L. Lin, T. Mihalisin, and X. Q. Wang, Magnetization and specific heat studies of Gd_2In, J. Appl. Phys. **79**, 5403 (1996).

[6] M. I. Ilyn, A. M. Tishin, K. A. Gschneidner Jr., V. K. Pecharsky, and A. O. Pecharsky, Magnetothermal properties of polycrystalline Gd_2In, Cryocoolers **11**, 457 (2002).

[7] A. Bhattacharyya, S. Giri, and S. Majumdar, Field induced sign reversal of magnetocaloric effect in Gd_2In, J. Magn. Magn. Mater. **324**, 1239 (2012).

[8] S. Tencé and B. Chevalier, Magnetic and magnetocaloric properties of $Gd_2In_{0.8}X_{0.2}$ compounds (X = Al, Ga, Sn, Pb), J. Magn. Magn. Mater. **399**, 46 (2016).

[9] F. Guillou, A. K. Pathak, D. Paudyal, Y. Mudryk, F. Wilhelm, A. Rogalev, and V. K. Pecharsky, Non-hysteretic first-order phase transition with large latent heat and giant low-field magnetocaloric effect, Nat. Commun. **9**, 2925 (2018).

[10] M. L. Fornasini, and S. Cirafici, Crystal structures of Eu_3Ga_2, EuGa, Eu_2In, EuIn, and $EuIn_4$, Z. Kristall. **190**, 295 (1990).

[11] P. Ehrenfest, Phasenumwandlungen im ueblichen und erweiterten Sinn, classifiziert nach den entsprechenden Singularitaeten des thermodynamischen Potentiales, Proceedings of the Koninklijke Nederlandse Akademie van Wetenschappen te Amsterdam **36**, 153 (1933).

[12] J. R. Salvador, F. Guo, T. Hogan, and M. G. Kanatzidis, Zero thermal expansion in YbGaGe due to an electronic valence transition, Nature (London) **425**, 702 (2003).

[13] S. Chatterjee, J. P. Ruf, H. I. Wei, K. D. Finkelstein, D. G. Schlom, and K. M. Shen, Lifshitz transition from valence fluctuations in $YbAl_3$, Nat. Commun. **8**, 852 (2017).

[14] O. D. McMasters, C. L. Nipper, and K. A. Gschneidner Jr., The ytterbium-indium system, J. Less-Common Metals **23**, 253 (1971).

[15] J. Rodríguez-Carvajal, Recent advances in magnetic structure determination by neutron powder diffraction, Physica B **192**, 55 (1993).

[16] J. Flahaut and F. Thévet, Filiation structurale des composés de formule générale AB_2: Etude comparée des types Co_2Si, Co_2P, $PbCl_2$, et SbSI, J. Solid State Chem. **32**, 365 (1980).

[17] R. D. Shannon, Revised effective ionic radii and systematic studies of interatomic distances in halides and chalcogenides, Acta Crystallogr. A **32**, 751 (1976).

[18] K. A. Gschneidner Jr. and L. R. Eyring, *Handbook on the Physics and Chemistry of Rare Earths* (Elsevier, Amsterdam, 1978), Vol. 1.

[19] D. H. Ryan, D. Paudyal, F. Guillou, Y. Mudryk, A. K. Pathak, and V. K. Pecharsky, The first-order magnetoelastic transition in Eu_2In: A ^{151}Eu Mössbauer study, AIP Adv. **9**, 125137 (2019).

[20] J. C. P. Klaasse, F. R. de Boer, and P. F. de Châtel, Systematics in intermetallic compounds containing intermediate-valent ytterbium, Physica B+C **106**, 178 (1981).

[21] M. Mitric, B. Antic, M. Balanda, D. Rodic, and M. Lj Napijalo, An x-ray diffraction and magnetic susceptibility study of $Yb_xY_{2-x}O_3$, J. Phys.: Condens. Matter **9**, 4103 (1997).

[22] See Supplemental Material at http://link.aps.org/supplemental/10.1103/PhysRevMaterials.4.104402 for details on the magnetic susceptibility of Yb_2In, powder-diffraction experiments on $Eu_{1.75}Yb_{0.25}In$ and $Eu_{2-x}Yb_xIn$ alloys and magnetic properties of $Eu_{2-x}Yb_xIn$ alloys. See also P. G. de Gennes, Sur les propriétés des métaux de terres rares, C. R. Acad. Sci. **247**, 1836 (1958).

[23] O. Stelmakhovych, B. Stelmakhovych, K. Uhlířová, S. Mašková, L. Havela, and Ya. Kalychak, $SmZn_{11}$-type derivative compound in the Yb-Zn-Al system: Crystal structure and magnetic properties, J. Solid State Chem. **184**, 1715 (2011).

[24] C. Kittel, *Introduction to Solid State Physics*, 7th ed. (John Wiley & Sons, Inc., New York, 1996).

[25] A. Bhattacharyya, S. Chatterjee, S. Giri, and S. Majumdar, Magnetotransport and magnetocaloric effect in Ho_2In, Eur. Phys. J. B **70**, 347 (2009).

[26] V. Singh, A. Bhattacharyya, S. Majumdar, and I. Dasgupta, A theoretical and experimental study of magnetism in Gd_2In, J. Appl. Phys. **111**, 053709 (2012).

[27] E. S. R. Gopal, *Specific Heats at Low Temperatures* (Springer, Plenum Press, New York, 1966).

[28] P. Kumar, K. G. Suresh, and A. K. Nigam, Magnetism, heat capacity, magnetocaloric effect and magneto-transport in R_2Al (R = Nd, Gd, Tb) compounds, J. Phys. D: Appl. Phys. **41**, 105007 (2008).

[29] D. T. K. Anh, G. Nakamoto, T. Tsuji, M. Kurisu, Y. Andoh, T. Tsutaoka, N. Achiwa, and S. Kawano, Magnetic, specific heat and powder neutron diffraction studies of Ho_2In, Physica B **381**, 132 (2006).

[30] A. Bhattacharyya, S. Chatterjee, S. Giri, and S. Majumdar, Magnetic anomaly and magnetocaloric effect in Dy_2In, J. Magn. Magn. Mater. **321**, 1828 (2009).

[31] C. D. Cao, R. Klingeler, H. Vinzelberg, N. Leps, W. Löser, G. Behr, F. Muranyi, V. Kataev, and B. Büchner, Magnetic anisotropy and ferromagnetic correlations above the Curie temperature in Eu_2CuSi_3 single crystals, Phys. Rev. B **82**, 134446 (2010).

[32] U. B. Paramanik, R. Prasad, C. Geibel, and Z. Hossain, Itinerant and local-moment magnetism in $EuCr_2As_2$ single crystals, Phys. Rev. B **89**, 144423 (2014).

[33] E. Mendive-Tapia, D. Paudyal, L. Petit, and J. B. Staunton, First-order ferromagnetic transitions of lanthanide local moments in divalent compounds: An itinerant electron positive feedback mechanism and Fermi surface topological change, Phys. Rev. B **101**, 174437 (2020).

[34] L. Jia, G. J. Liu, J. R. Sun, H. W. Zhang, F. X. Hu, C. Dong, G. H. Rao, and B. G. Shen, Entropy changes associated with the first-order magnetic transition in $LaFe_{13-x}Si_x$, J. Appl. Phys. **100**, 123904 (2006).

[35] N. Kamali Sarvestani, S. Ahmad Ketabi, and A. Yazdani, Electro-mechanical character of Gd and Gd_2In and possibility of a Kondo-like behavior in Gd_2In, J. Alloys Compd. **613**, 62 (2014).

[36] K. A. Gschneidner Jr., Systematics of the intra-rare-earth binary alloy systems, J. Less. Common Metals **114**, 29 (1985).

[37] K. A. Gschneidner Jr., V. K. Pecharsky, and A. O. Tsokol, Recent developments in magnetocaloric materials, Rep. Prog. Phys. **68**, 1479 (2005).

[38] B. P. Alho, P. O. Ribeiro, P. J. von Ranke, F. Guillou, Y. Mudryk, and V. K. Pecharsky, Free energy analysis of the non-hysteretic first order phase transition of Eu_2In (unpublished).

[39] V. K. Pecharsky, K. A. Gschneidner Jr., A. O. Pecharsky, and A. Tishin, Thermodynamics of the magnetocaloric effect, Phys. Rev. B **64**, 144406 (2001).